

RESEARCH

Open Access

# Characterization of argon/air atmospheric pressure capacitively coupled radio frequency dielectric barrier discharge regarding parasitic capacitor at 13.56 MHz

Farshad Sohbatzadeh<sup>\*</sup>, Saeed Mirzanejhad, Hoda Mahdavi and Zahra Omid

## Abstract

In this paper, uniform argon glow discharge at atmospheric pressure in a diffuse mode driven by a 300-W radio-frequency (13.56 MHz) power supply based on dielectric barrier discharge was investigated. In this work, the effect of the parasitic capacitor on the electrical characteristics of the capacitively coupled atmospheric pressure plasma was investigated. It was revealed that more than half of the RF current is parasitic in our system as a characteristic of the capacitively coupled plasma. It was also proved that the discharge resistance and sheath capacitance increase at higher input powers while the impedance decreases. In order to recognize plasma, optical emission spectroscopy apparatus was used. Argon, oxygen, copper, and nitrogen spectrum lines were diagnosed. The plasma gas temperature and electronic excitation temperature were investigated showing a non-equilibrium discharge.

## Background

Nowadays, plasma is used in much wider fields including microelectronics, biomedical, and especially material processing such as surface modification, cleaning, and etching. Since the capital costs of the complicated vacuum systems are very high and the geometrical size of the treated materials are limited by the vacuum chamber volume, different kinds of atmospheric pressure cold discharge plasma sources have been developed in a wide range of frequency from dc to microwave, or in a short pulse. A microwave and RF plasma torch, capacitively coupled, atmospheric pressure plasma, are well-known examples of atmospheric plasma sources [1-8]. Due to the many unique features such as large volume, stability, low gas temperature, and high concentration of chemically active species, in recent years, atmospheric pressure glow discharges driven by RF power supply have commended much attention [9]. Their applications include surface cleaning and activation, film deposition, and decontamination of chemical or biological warfare agents, etc. [10,11]. In some application areas of

atmospheric plasmas, especially for surface modification of large-area materials such as fabrics and polymers, having an area with high uniformity in plasma parameters is one of the most important requirements that the plasma source should satisfy. Atmospheric dielectric barrier discharges (DBDs) are typically used for activation and modification of surfaces, sterilization, bioactivation, the deposition of coating barriers, synthesis, and decomposition processing [12,13]. Atmospheric DBDs have the advantage that at relative high pressure, cold but chemically active plasma is created. Cold plasmas are preferable since they are more generally usable for surface handling. With this motivation, we investigated a continuous, uniform plasma source with atmospheric pressure using RF power supply at 13.56 MHz. We employed a DBD-type hardware arrangement, which consists of a dielectric material covering on one of the electrodes, limiting the over current and assist, and producing stable, uniform glow plasma at atmospheric pressure. A parallel-plate DBD system was used to produce glow discharge using argon/air gases at atmospheric pressure. The measurements, together with analysis of the equivalent circuit of the apparatus, revealed that the RF current substantially involves as the parasitic one,

<sup>\*</sup> Correspondence: f.sohbat@umz.ac.ir  
Department of Atomic and Molecular Physics, Science Faculty, University of Mazandaran, Babolsar 47416-95447, Iran

which originates from the displacement current flowing through the parasitic capacitor. This, in turn, gives rise to energy loss.

This paper is organized as follows: 'Experimental set up' section, 'Methods' section which describes the basic discharge parameters such as RF voltage, RF current, and phase angle between voltage and current and finally, the 'Conclusions' section.

### Experimental set-up

The atmospheric pressure glow discharge was produced between two planar circular electrodes. One electrode was connected to the RF power supply through an impedance matching network. The other electrode was grounded. The surface area of each electrode was  $678 \text{ mm}^2$ , and the spacing between two electrodes was set to be 0.8 mm. A circular glass which is used as the dielectric barrier layer with the 0.92 mm thickness covered the grounded electrode. Argon/air (99:1%) as the plasma forming gases with the flow rate of 5 l/min were supplied in to the discharge region through a gas hole array. The 13.56 MHz power was supplied by an AG0313, 300 W power supply (T&C Power Conversion Inc., Rochester, NY, USA). The RF power was coupled from the generator

to the electrode, using 50  $\Omega$  coaxial cable and a matching network (T&C Power Conversion, model ATN-10). The transmitted and reflected powers were monitored using an RF-directional power meter (model 4410-A Thruline Wattmeter, Bird Electronic Corporation, Solon, OH, USA). The experimental discharge structure and the measurement instrumentations are shown in Figure 1. After gas electrical breakdown, the matching network adapted the electrode impedance to 50  $\Omega$ ; consequently, the reflected power was less than 2%. Diagnostics of the produced plasma were performed by optical emission spectroscopy (OES), and the results were used to calculate the average electron excitation temperature and electron density. A quartz optical fiber, connected to a spectrometer (model S-100, Solar Laser Systems Ltd, Minsk, Belarus), was held at some distance of the plasma plume. The resolution power of the spectrometer is about 1 nm and covers UV-visible and near infrared wavelengths from 190 to 1,100 nm. The electrical characteristics of the produced plasma were also measured by simultaneously measuring the RF voltage and current across the electrodes. The measurements were made using a high voltage probe (Tektronix P6015A Tektronix Inc., Beaverton, OR, USA) and a

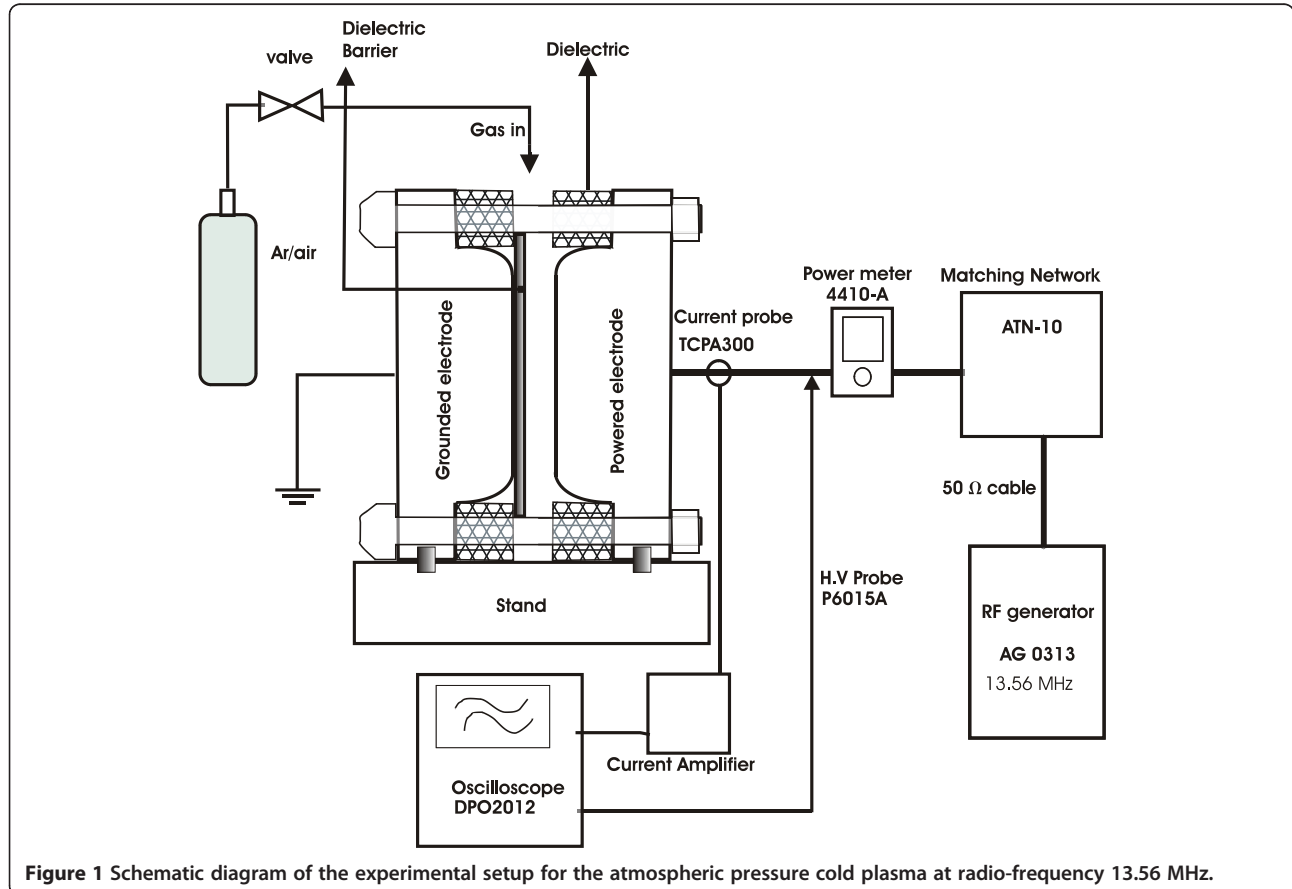


**Figure 1** Schematic diagram of the experimental setup for the atmospheric pressure cold plasma at radio-frequency 13.56 MHz.

current probe (Tektronix TCPA-300), and the results were recorded on a digital oscilloscope (Tektronix DPO-2012).

### Methods

The electrical characteristics of the atmospheric pressure glow discharge can be identified by the relations between voltage, current, and phase angle. In this configuration, the phase difference between RF voltage ( $V_0(t)$ ) and RF current ( $I_0(t)$ ) is nearly  $90^\circ$  before gas breakdown. It indicates that the equivalent circuit of the system is purely capacitive and the load impedance is equal to the absolute value of the reactance. As shown in Figure 2, the phase difference between the RF voltage and current decreases and becomes smaller by increasing input power after gas breakdown. This indicates that the system tends to be resistive at relatively high input power. Figure 3 shows the behavior of the voltage-power ( $V$ - $P$ ) of the gas gap. Curve I indicates the  $V$ - $P$  before gas breakdown. After breakdown, there is a transition from curve I to III, where an abrupt decrease in voltage takes place. By reducing the applied power,  $V$ - $P$  characteristic curve III is obtained showing less voltage on the electrode comparing to curve I. As can be seen, there is hysteresis in the  $V$ - $P$  curve.

Figure 4 shows the  $V$ - $I$  characteristic curve for the plasma gap. Path I denotes  $V$ - $I$  before gas breakdown and path II denotes that for the gas discharge while the power is reduced gradually. It is worthy of note that before gas breakdown, the RF current totally appears in displacement current. The contribution of displacement current is also significant, after gas breakdown.

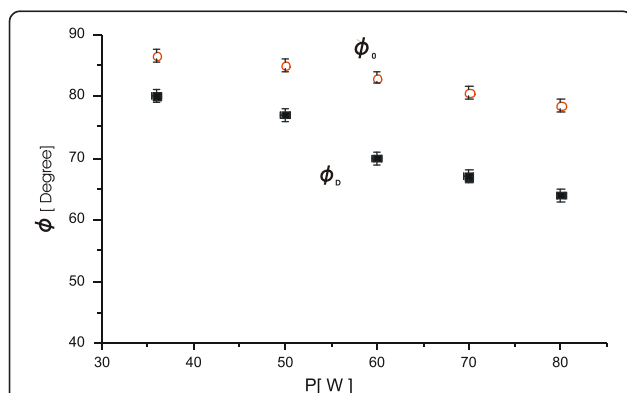


**Figure 2** Variation of phase angle difference between voltage and current. Variation of phase angle difference between voltage and current as a function of input power for argon/air with flow rate of 5 l/min. The white circles are for phase difference  $\phi_0$  between RF voltage  $V_0(t)$  and RF current  $I_0(t)$ . The black squares are for phase difference  $\phi_d$  between discharge voltage  $V_d(t)$  and discharge current  $I_d(t)$ .

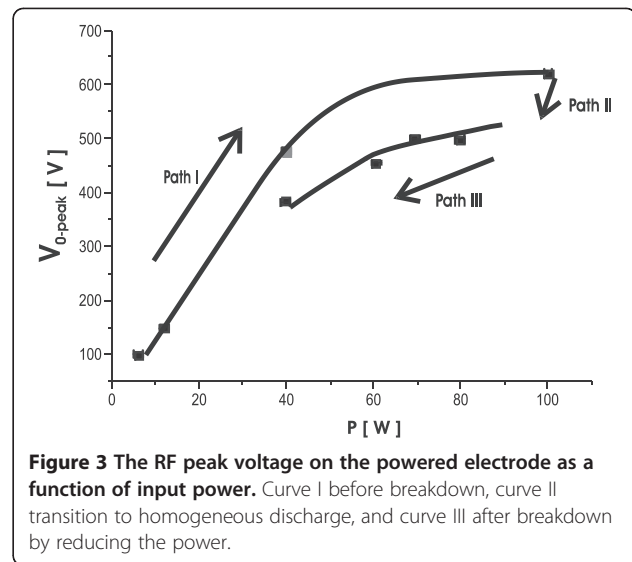


**Figure 3** The RF peak voltage on the powered electrode as a function of input power. Curve I before breakdown, curve II transition to homogeneous discharge, and curve III after breakdown by reducing the power.

### Equivalent circuit

In order to recognize the plasma parameters, we made an equivalent electric circuit based on measured electrical parameters [14]. As can be seen in Figure 5, there is a parasitic capacitor,  $C_{para}$ , which equals to 1.52 PF in parallel to the plasma impedance  $Z_{plasma}$ . It influences the discharge voltage ( $V_d$ ) and discharge current ( $I_d$ ). The discharge voltage  $V_d$  is equal to the total RF voltage  $V_0$ . On the other hand, the discharge current  $I_d$  is calculated by

$$I_d = \sqrt{(\omega C_{para} V_0)^2 + I_0^2 - 2\omega C_{para} V_0 I_0 \sin \phi_0} \quad (1)$$

where  $\omega$  is the angular frequency of the RF field,  $V_0$  and  $I_0$  are the RF peak voltage and current, and  $\phi_0$  is the phase difference between RF voltage ( $V_0(t)$ ) and RF current ( $I_0(t)$ ). Equation 1 predicts that the discharge current depends strongly on the parasitic capacitor  $C_{para}$ . In our system, the parasitic capacitor makes the RF

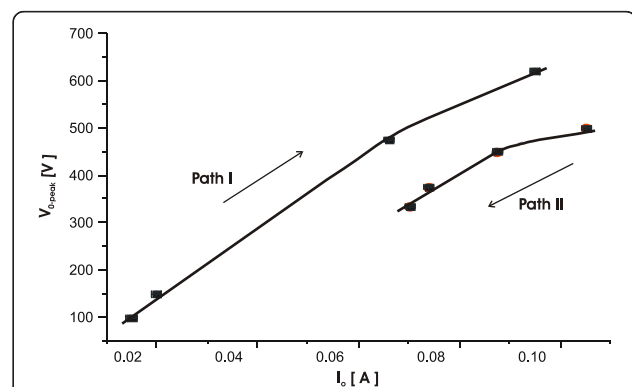
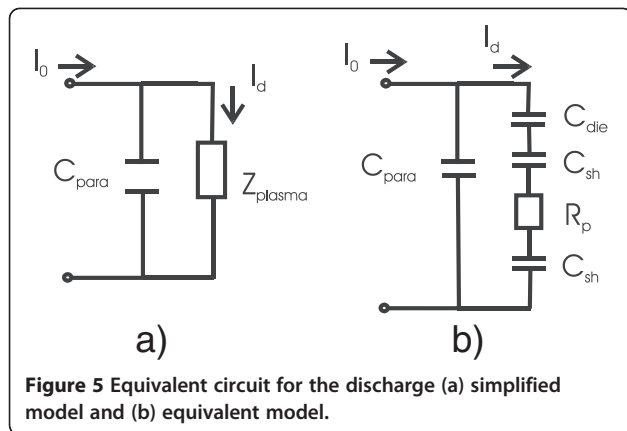


**Figure 4** The voltage-current characteristic curve before and after gas breakdown. Path I: before gas breakdown and path II: after gas breakdown.



current to form a parasitic current significantly, which gives rise to energy losses. The current density of the discharge  $J_d$  is given by

$$J_d = \frac{I_d}{A_{plasma}}, \quad (2)$$

where  $A_{plasma}$  is the discharge cross section. The magnitude of the plasma impedance  $|Z_{plasma}|$  and the phase difference  $\phi_d$  between discharge voltage ( $V_d(t)$ ) and discharge current ( $I_d(t)$ ) are given respectively as

$$|Z_{plasma}| = \frac{1}{\sqrt{(\omega C_{para})^2 + \left(\frac{I_0}{V_0}\right)^2 - 2\omega C_{para} \frac{I_0}{V_0} \sin\phi_0}}, \quad (3)$$

$$\phi_d = \cos^{-1}\left(\frac{I_0}{I_d} \cos\phi_0\right), \quad (4)$$

Equation 3 shows the effect of the parasitic capacitor on the phase difference between discharge voltage  $V_d(t)$  and current  $I_d(t)$ , i.e., reduces  $\phi_d$  such that  $\phi_d < \phi_0$ . This behavior is illustrated in Figure 2.

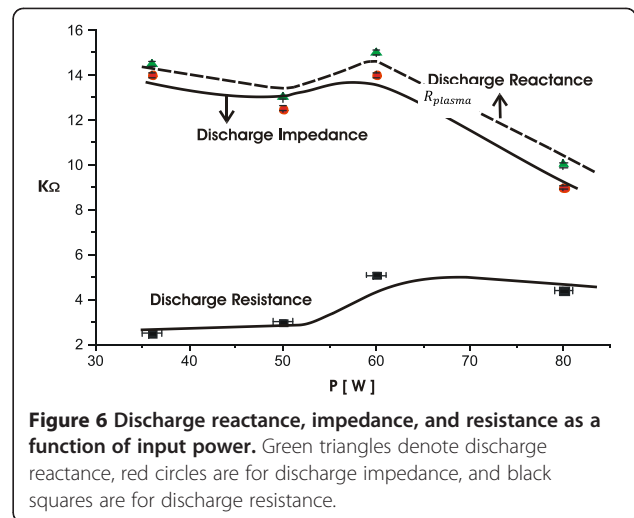
To model the RF discharge electrically, we substituted the dielectric by a capacitor  $C_{diel}$ , positive ion sheath by  $C_{sh}$  and the plasma column by a resistor  $R_p$ . In this model  $C_{diel}$ ,  $C_{sh}$ , and  $R_p$  are in series. The discharge resistance, reactance, and sheath capacitance can be evaluated by

$$R_p = \cos\phi_d |Z_{plasma}| \quad (5)$$

$$x_p = \sin\phi_d |Z_{plasma}| \quad (6)$$

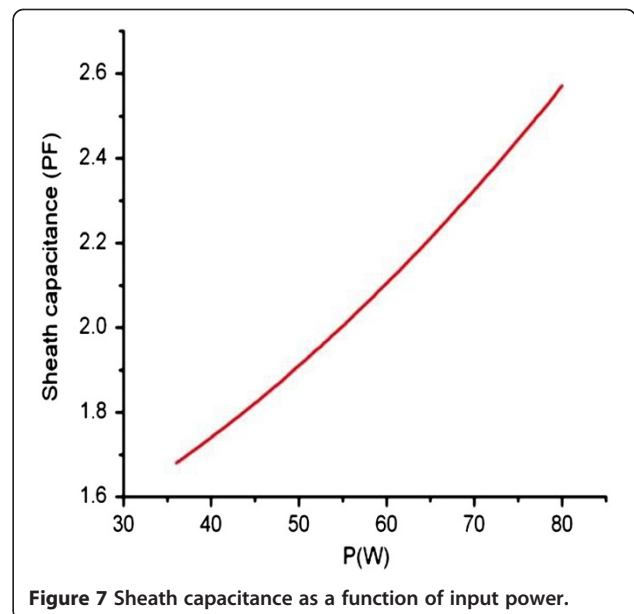
$$C_{sh} = \frac{2}{\omega |Z_{plasma}| \sin\phi - \frac{1}{C_{diel}}} \quad (7)$$

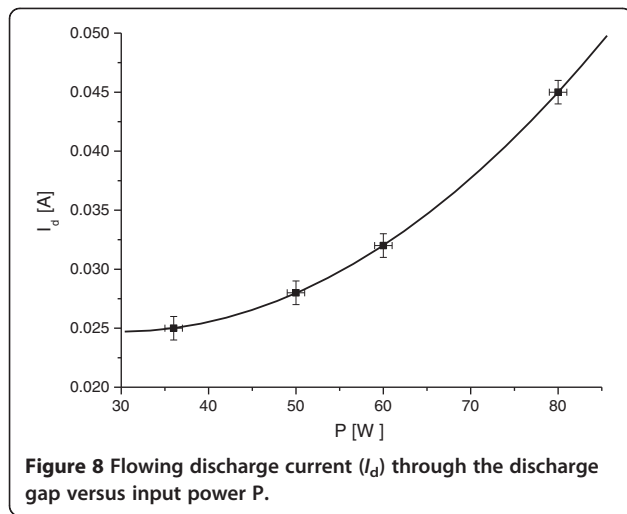
The evaluated curves for these parameters are shown in Figures 6 and 7. As shown in Figure 6, by increasing input power, both the reactance and impedance decrease



while the discharge resistance increases. At about 60 W of input power, there is an increase in the discharge resistance. This can be attributed to the increase in gas temperature, since there was no installed any cooling apparatus in our system. Figure 7 indicates the sheath capacitance curve versus RF power. It is seen that sheath capacitance increases by increasing power. It means that the thickness of the positive space-charge layers near the electrode decreases at higher input powers.

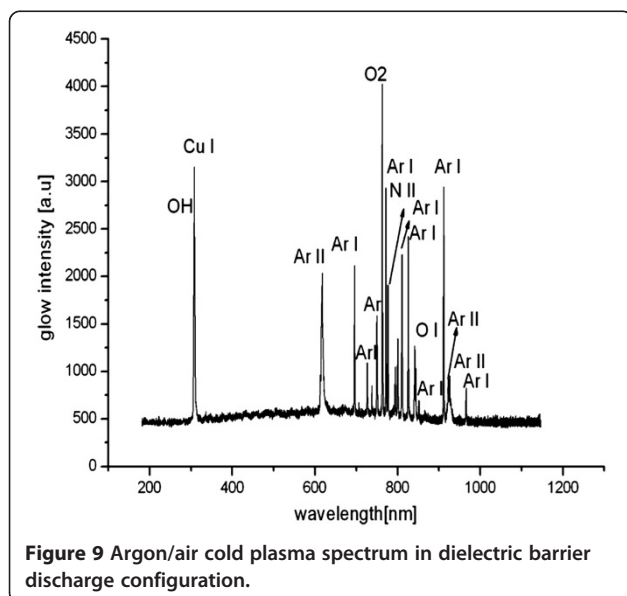
Figure 8 shows the maximum discharge current as a function of input power. It is seen that by increasing the RF power, the discharge current increases, although more than half of the RF current passes through the parasitic capacitor  $C_{para}$ . For example, at input powers of 80 and 60 W, the ratio  $\frac{I_d}{I_0}$  is 0.429 and 0.433, respectively.





### Optical emission spectroscopy

We used OES for recognizing the discharge species. Figure 9 shows the spectra intensities measured by the spectrometer. By applying RF power to the electrode, gas breakdown occurs, and charged particles such as electrons, ions, and neutral atoms are produced. The ionized state in the gas builds up until it reaches appreciable values, and plasma species radiate in different wavelengths. These wavelengths are related to the atomic argon (Ar(I)) and ionized argon with one degree of ionization (Ar(II)). Because of the powered electrode sputtering by the high energy ions, atomic copper (Cu(I)) spectrum line is distinguished. Spectrum lines 777 and 844 nm are attributed to the atomic oxygen. In this experiment, the spectrum line 306 nm can be attributed



to OH radical due to humidity of our laboratory. Due to the discharge gas composition, N(II) spectrum line is also distinguished.

Having the spectrum lines of the discharge, one can evaluate the electronic excitation temperature and electron density by using Boltzmann plot. For plasma in local thermodynamic equilibrium, the energy level relative populations of the species is given by the Boltzmann distribution law [15] as

$$\frac{n_k}{n_0} = \frac{g_k}{g_0} e^{-\frac{E_k}{k_B T}} \quad (8)$$

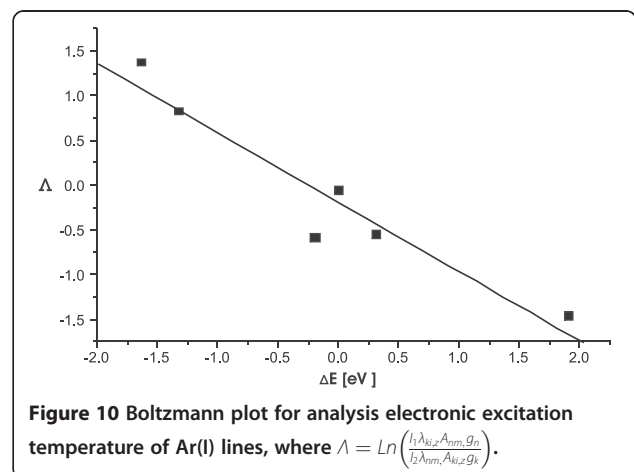
where,  $n_k$ , and  $n_0$  are the number density of the particles in the excited and ground state, respectively.  $g_o$  and  $g_o$  are the statistical weights corresponding to the energy levels,  $E_k$  is the excitation energy of the excited state  $k$ ,  $k_B$  is the Boltzmann constant and  $T$  is the excitation temperature. The intensity of the emission line corresponding to the transmission between the upper energy level  $k$  and the lower energy level  $L$  is given by

$$I_{kl} = k N_k A_{kl} h \nu_{kl}, \quad (9)$$

where  $k$  is an instrumental function related to the spectrometer detect ability,  $N_k$  is the number of atoms in upper state  $k$ ,  $A_{kL}$  is the number of transitions per unit time,  $h\nu_{kL}$  is the quantum of the radiated energy. Using Equations 8 and 9, the intensity ratio between two lines of the same species of ionization stage  $Z$  in terms of wavelength is expressed as

$$\frac{I_1}{I_2} = \left( \frac{g_{k,z}}{g_{n,z}} \right) \left( \frac{A_{ki,z}}{A_{nm,z}} \right) \left( \frac{\lambda_{nm,z}}{\lambda_{ki,z}} \right) e^{-\frac{E_{k,z} - E_{n,z}}{k_B T}}, \quad (10)$$

where  $I_1$  is the line intensity from the  $k$ - $i$  transition, and  $I_2$  is that from the  $n$ - $m$  transition. Figure 10 shows the Boltzmann plot from the intensities of argon atomic lines, the slope gives the average electronic excitation



temperature  $T = 0.74$  eV. To plot Equation 10, the NIST atomic database was used [16]. In order to check the plasma gas temperature  $T_g$ , the flow rate of the flowing gas was increased to about 10 l/min in which the plasma plume emerged from the electrode gap. The temperature of the effluent plume was measured by a thermometer. It was proved that the plasma gas temperature is a function of the applied RF power and was measured to be about 373 K at 100 W RF input power.

The electron density using atomic and ionic spectral lines emitted from the plasma can be determined from the Saha-Boltzmann equation as [17,18]

$$n_e = \frac{6.04 \times 10^{21} I_z^*}{I_{z+1}^*} T^{\frac{5}{2}} \exp \left[ \frac{-E_{k,z+1} + E_{k,z} - \chi_z}{k_B T} \right] \text{cm}^{-3} \quad (11)$$

where  $I_z^* = I_z \lambda_{ki,z} / g_{k,z} A_{ki,z}$  and  $\chi_z$  is the ionization energy of the species in the ionization stage  $Z$ . We considered two intensity ratios, 800 nm Ar(I) and 922 nm Ar(II) as well as 811 nm Ar(I) and 922 nm Ar(II). The arithmetic mean of the two values of  $n_e$  is represented as the average value of the electron density and is estimated to be  $n_e = 1.92 \times 10^{12} \text{ cm}^{-3}$ .

## Conclusions

An RF discharge maintained between two planar electrodes was investigated experimentally. The voltage, current, and related phase difference were measured. An equivalent circuit model was made to consider the discharge. It was revealed that the discharge current depends strongly on the parasitic capacitor  $C_{\text{para}}$ . It makes the RF current to compose parasitic current significantly which gives rise to energy losses. The analysis suggests keeping parasitic capacitor as small as possible in plasma head designs. It was also concluded that the discharge tends to be resistive at relatively higher input powers. Argon, oxygen, copper, and nitrogen spectrum lines were diagnosed in spectroscopy measurement of the plasma which revealed one degree of ionization. Because of electrode sputtering caused by high energy ions, copper spectrum lines also appeared. Based on spectroscopy results, the device could atomize the molecules of oxygen converting to O(I). Atomic oxygen is very reactive. It can form a polar bond on the surfaces which leads to hydrophilicity. It can disinfect biological agents via cell wall peroxidation. We determined the average electronic excitation temperature using Boltzmann plot method made from Ar(I) spectral lines which was about 0.74 eV, and the average value of the electron density from the Saha-Boltzmann equation to be about  $1.92 \times 10^{12} \text{ cm}^{-3}$ . The plasma gas temperature was about 373 K at 100 W RF input power. The relatively low gas temperature makes the produced plasma so useful in material processing.

## Competing interests

The authors declare that they have no competing interests.

## Authors' contributions

All authors read and approved the final manuscript.

## Acknowledgement

Authors would like to thank to the Research and Technology deputy of University of Mazandaran for partial support of this work (grant number 379/D/33).

Received: 4 August 2012 Accepted: 20 October 2012

Published: 22 November 2012

## References

1. Li, HP, Li, G, Sun, WT, Wang, S, Bao, CY, Wang, L, Huang, Z, Ding, N, Zhao, H, Xing, XH: Radio-frequency atmospheric-pressure glow Discharge; producing methods, characteristics and applications in bio-medical fields. *Appl. Phys.* **982**, 584 (2008)
2. Moon, SY, Choe, W, Kang, BK: A uniform glow discharge plasma source at atmospheric pressure. *Appl. Phys. Lett.* **84**, 188 (2003)
3. Li, B, Chen, Q, Liu, ZW: A large gap of radio frequency dielectric barrier atmospheric pressure glow discharge. *Appl. Phys. Lett.* **96**, 041502 (2010)
4. Shi, JJ, Liu, DW, Kong, MG: Mitigating plasma constriction using dielectric barriers in radio-frequency atmospheric pressure glow discharges. *Appl. Phys. Lett.* **90**, 031505 (2007)
5. Park, J, Henins, I, Herrmann, HW, Selwyn, GS: Gas breakdown in an atmospheric pressure radio-frequency capacitive plasma source. *J. Appl. Phys.* **89**, 15 (2001)
6. Shi, JJ, Liu, DW, Kon, MG: Plasma stability control using dielectric barriers in radio-frequency atmospheric pressure glow discharges. *Appl. Phys. Lett.* **89**, 081502 (2006)
7. Simor, M, Rahel, J, Vojtek, P, Cernak, M, Brablec, A: Diagnostics of atmospheric pressure surface plasmas in argon. *Appl. Phys. Lett.* **81**, 2716 (2002)
8. Moon, SY, Rhee, JK, Kim, DB, Choe, W:  $\alpha$ ,  $\gamma$ , and normal, abnormal glow discharge modes in radio-frequency capacitively coupled discharges at atmospheric pressure. *Phys. Plasmas* **13**, 033502 (2006)
9. Shang, W, Wang, D, Zhang, Y: Radio frequency atmospheric pressure glow discharge in modes between two coaxial electrodes. *Phys. Plasmas* **15**, 093501–093503 (2008)
10. Shafer, J, Foest, R, Ohl, A, Weltmann, KD: Miniaturized Non-thermal atmospheric pressure plasma jet-characterization of self-organized regimes. *Plasma Phys. Control. Fusion.* **51**, 1 (2009)
11. Li, G, Li, HP, Sun, WT, Wang, S, Tian, Z, Bao, CY: Discharge features of radio-frequency, atmospheric-pressure cold plasmas under an intensified local electric field. *J. Phys. D: Appl. Phys.* **41**, 202001 (2008)
12. Burn, KTAL: Temperatures in dielectric barrier gas discharges for surface treatment. *Contrib. Plasma Phys.* **45**, 54 (2005)
13. Kogelschatz, U: Dielectric-barrier discharges: their history, discharge physics, and industrial applications. *Plasma Chem Plasma P* **23**, 1 (2003)
14. Haslinger, S, Laimer, J, Stori, H: Stability conditions of argon and helium gas mixtures in an atmospheric pressure plasma jet. *Vacuum* **82**, 142 (2008)
15. Payling, R, Jones, D, Bengtson, A: *Glow Discharge Optical Emission Spectroscopy*. Wiley, Chichester (1997)
16. Kramida, A, Ralchenko, Y, Reader, J, NIST ASD Team: NIST Atomic Spectra Database (ver. 5.0). National Institute of Standards and Technology, Gaithersburg (2012). Available: <http://physics.nist.gov/asd>
17. Griem, HR: *Principles of Plasma Spectroscopy*. Cambridge University Press, Cambridge (1997)
18. Unnikrishnan, VK, Alti, K, Kartha, VB, Santhosh, C, Gupta, GP, Suri, BM: Measurements of plasma temperature and electron density in laser-induced copper plasma by time-resolved spectroscopy of neutral atom and ion emission. *Pramana-J. Phys.* **74**, 983 (2010)

doi:10.1186/2251-7235-6-32

Cite this article as: Sohbatzadeh et al.: Characterization of argon/air atmospheric pressure capacitively coupled radio frequency dielectric barrier discharge regarding parasitic capacitor at 13.56 MHz. *Journal of Theoretical and Applied Physics* 2012 **6**:32.